J Digit Imaging
DOI 10.1007/s10278-011-9448-0

Influence of Image Metrics When Assessing Image Quality from a Test Object in Cardiac X-ray Systems: Part II

Roberto Sanchez · Eliseo Vano · Carlos Ubeda · Jose M. Fernandez · Stephen Balter · Bart Hoornaert

Abstract The images generated in modern IC laboratories are created with high-quality standard (1,024×1,024 pixels and 10–12 bits/pixel) enabling cardiologists to perform interventions in the best conditions. But these images are in most of the cases archived in a basic quality standard (512×512 pixels and 8 bits/pixel). The purpose of this work is to complete the research developed in a previous paper and analyze the influence of the matrix size and the bit depth reduction on the image quality acquired on a polymethylmethacrylate (PMMA) phantom with a test object. The variation in contrast-to-noise ratio (CNR) and high contrast spatial resolution (HCSR) were investigated when the matrix size and the bit depth were independently modified for different phantom thicknesses. These two image quality parameters did not suffer noticeable alterations under bits depth reduction from 10 to 8 bits. Such a result seems to imply that bits depth reduction could be used to reduce file sizes with a suitable algorithm and without losing perceptible image quality information. But when the matrix size was reduced from 1,024×1,024 to 512×512 pixels, a reduction from 17% to 25% in HCSR was noticed when changing phantom thickness, and an increase of 27% in CNR was observed. These findings should be taken into account and it would be wise to conduct further investigations in the field of clinical images.

Keywords Image quality · Test object · Matrix size · Bits depth · Image metrics · Cardiology

R. Sanchez · J. M. Fernandez
Medical Physics, Hospital Clinico San Carlos, Instituto de Investigación Sanitaria del Hospital Clínico San Carlos (IdISSC), 28040 Madrid, Spain

E. Vano (✉)
Radiology Department,
Complutense University and San Carlos Hospital,
28040 Madrid, Spain
e-mail: eliseov@med.ucm.es

C. Ubeda
Clinical Sciences Department, Faculty of the Science of Health,
Tarapaca University,
Arica, Chile

S. Balter
Columbia University Medical Center,
627 West 165th Street,
New York, NY 10032, USA

B. Hoornaert
PhilipsHealthcare, BU Interventional X-Ray, R&D,
5680 DA Best, The Netherlands

Published online: 06 January 2012

Introduction

In interventional cardiology (IC) suites, images are commonly stored with DICOM (Digital Imaging and Communications in Medicine) high-resolution standard for cardiac applications of 1,024×1,024 pixels and 10 or 12 bits at the local hard drive to be later transferred to PACS (Picture and Archiving Communication System) or other removable media (DVD, CD, etc.). They are finally saved in the basic archiving standard for cardiology of 512× 512 pixels and 8 bits: this format used since the early 1990s provides the smallest dataset with clinically acceptable images [1]. Image receptors and local fluoroscopic storage now allow the acquisition and storage of images at the spatial and bit depth resolutions described in this paper. But data sets stored on removable media or on PACS systems are still usually in the original DICOM format.

The amount of information generated at an IC department can be huge, which makes storage management difficult. For example, a typical diagnostic series of 6 s with15 frames

s^{-1} cine acquisitions can reach up to 50 MB of digital data (without compression). Image compression has been explored as a means of increasing network speed and reducing the cost of archiving large image data sets. To achieve size reduction, there are two methods currently used, lossless and lossy compression [2–6].

Chuang and Huang [7] have demonstrated that if an appropriate algorithm is used and depending on the quantity of image noise, it is possible to transform the bit depth from 10 to 8 bits grey scale with a minimal loss of information. But image degradation has hardly been investigated when image metrics are reduced from 1,024×1,024 and 12 bits matrix (as acquired in the new cardiac systems) to 512×512 and 8 bits (as archived in most laboratories).

This paper is Part II of the research recently published by Vano et al. [8], in which the effect of reducing image metrics in Siemens systems was discussed and to split the influence of bits depth and matrix size, was then not feasible because of software limitations. Therefore, the aim of the present work is to analyze the impact of the different metrics on the image quality of a test object, mostly the effect of the matrix size but also of the bit depth with the Philips picture archiving system in cardiology. In this paper, considered as the follow-up of the previous one, the effect of matrix size reduction on image quality and bits depth has been investigated independently.

Materials and Methods

In this evaluation, we have used a methodology similar to the one described by Vano et al. [8], but with some differences as to the X-ray unit and the definition of some quality image parameters. The cardiovascular X-ray system used for this evaluation: a Philips AlluraXper FD10 (http://www.healthcare.philips.com) equipped with a 19×18 cm^2 flat detector (FD), a pixel size of 184 μm has a nominal resolution of 1,024×1,024 pixels. Depending on the field size used, it can display images in three different formats: 25 cm (960×960 pixels), 20 cm (720×720 pixels) and 15 cm (600×600 pixels), all of them occupying 1,024×1,024 pixels×10 bits in memory. In this experiment, we used the 25-cm format. From now on and even though the real image size is slightly smaller, the nominal value of 1,024 or 512 will be used to describe the image resolution.

The geometrical setup described in detail by Vano et al. [8] simulated clinical conditions and used a polymethylmethacrylate (PMMA) phantom. The PMMA phantom was always positioned at the isocenter with thicknesses of 16, 20, 24 and 28 cm and source-to-phantom distances from 68.5 to 62.0 cm depending on phantom thickness. The image detector was situated about 15 cm from phantom and according to variation in phantom thicknesses was located at distances from focus from 98 to 104 cm. A test object (TO) TOR 18-FG (http://www.leedstestobjects.com) was positioned in the middle of the PMMA phantom.

The images for this experiment were acquired in cine mode, with pulse rate of 15 frames s^{-1} and 25 cm (diagonal dimension) of the field of view (FOV) at the FD. A plane-parallel ionization chamber (model 20×6–60) with a 2026 C radiation meter from RadCal (http://www.radcal.com) in contact with the PMMA plates was used to measure Entrance Surface Air Kerma ($K_{a,e}$) with backscatter (BS) [9]. The ionization chamber is present in the recorded images together with the TO because the $K_{a,e}$ measurements and the acquisition of the images were made simultaneously.

We also measured air kerma (AK) without backscatter [9] at the entrance of the FD using an Unfors Xi multimeter (http://www.unfors.com/products.php). The detector probe of this device is radio-opaque and special attention was paid to ensure that its position on the FD periphery remained unchanged during all the experiment and that the automatic exposure settings were unaltered by the probe presence. So, when comparing measured dose values with nominal ones, we have to take into account that differences could be affected by a lack of uniformity of the radiation field.

The TO contains a set of circles of equal size (8 mm), but different thickness producing a contrast range for low-contrast threshold evaluation purposes and a set of lead bar patterns for high-contrast spatial resolution (HCSR). The image quality can be evaluated by simply counting the number of low-contrast details detected and the number of bar patterns resolved by several experienced observers (subjective method) in a suitable display device, or measuring mean values and standard deviation (SD) in the appropriate regions of interest (ROIs) of the TO.

The imaging system permitted to archive the TO images with four different metrics. The acquisition was first performed in 1,024×1,024 matrix size, 16 bits allocated and 10 bits stored format. Then the images were exported to the other three different formats: 1,024×1,024 matrix size, 8 bits allocated and 8 bits stored, 512×512 matrix size, 16 bits allocated and 8 bits stored or to the basic DICOM resolution standard in cardiology of 512×512 matrix size, 8 bits allocated and 8 bits stored.

The DICOM images acquired in cine mode were analyzed using Osiris software (version 4.19; http://www.sim.hcuge.ch/osiris/). The numerical image quality evaluation was always performed on three consecutive images for each series located at sequential positions 10, 12 and 15 so as to avoid stability problems likely to occur in the first images of the series. On each image, the mean value and SD in different ROIs were analyzed and for each series, we calculated the mean values and the higher SD of the three images. The ROIs sizes were larger than 150 pixels in the case of the matrix size of 512×512 and larger with the images of 1,024×1,024.

The image quality was analyzed using the mean values and SD of low-contrast circles and the HCSR groups. The analysis of the image quality was achieved as described by Vano et al. [8] through contrast-to-noise ratio (CNR), also known as differential signal-to-noise (dSNR) [10–13], and a parameter defined to measure the HCSR.

These numerical parameters are defined as (Fig. 1):

$$\mathrm{dSNR} = \frac{|\mathrm{BG} - \mathrm{ROI}|}{\sqrt{\frac{\left(\mathrm{SD}_1^2 - \mathrm{SD}_2^2\right)}{2}}} \quad (1)$$

$$\mathrm{HCSR} = \frac{|\mathrm{SD}_4 - \mathrm{SD}_3|}{\mathrm{ROI}_3} \quad (2)$$

where

BG is the background value — in our case, the mean value of the pixel content in a rectangular region of interest (ROI 2) near the low contrast circle number 3 and of the same size as the ROI selected from inside the circle.

ROI is the mean value of the pixel content in a rectangular region of interest (ROI 1) inside the circle number 3.

SD_1 is the corresponding standard deviation for the pixel content in the selected ROIs, inside circle number 3.

SD_2 is the corresponding standard deviation for the pixel content in the selected ROIs, outside circle number 3.

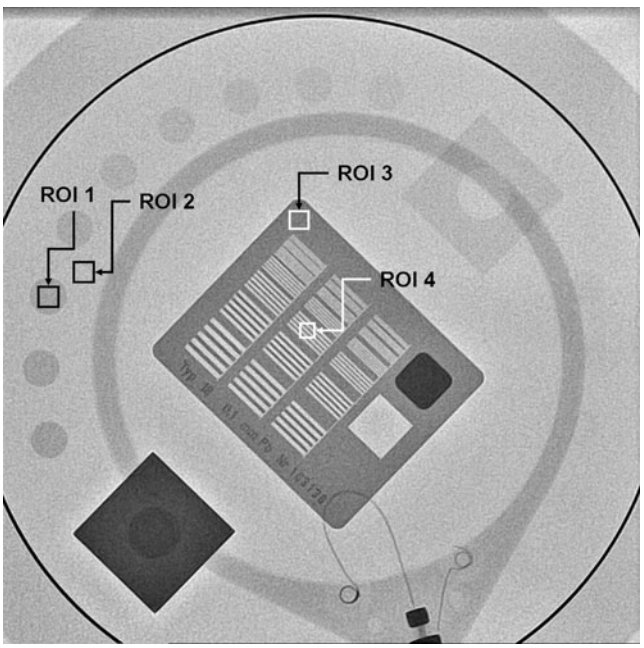

Fig. 1 Example of one of the images obtained and how its numerical evaluation was performed. Image corresponds to cine mode, 1024×1024 matrix size, 10 bits grey scale and FOV 25 cm, PMMA thickness 16 cm. ROI 1 used for the "signal" and ROI 2 for the background; ROIs 3–4 used to evaluate HCSR parameter

ROI_3 and SD_3 are the average and the standard deviation for the pixel content in the ROI 3 (Fig. 1), selected in the periphery of the HCSR groups.

SD_4 is the standard deviation for the pixel content in the ROI 4 (Fig. 1), inside the eighth group (arbitrary election to facilitate the numerical evaluation) in the central grid of the TO.

The definition of the HCSR parameter presented here has been normalized to ROI_3. This allows to rescale the parameter values and to make them relatively independent of pixel absolute value due to bits depth; pixel values and their SD would otherwise be different in part because of the different scale. The relationship between the parameter value and the results of a visual inspection is sometimes difficult to assess, but as HCSR parameter decreases it is expected that the results of visual inspection get worse. So this method has the advantage of evaluating the parameter without the subjective variations of the observers.

Differences between our dependent (normally distributed) groups of parameters (related to the image quality) were tested for significance with the ANOVA test and post-hoc analysis (Tukey's test). Values of p are reported to describe the results; those with $p<0.05$ were considered statistically significant. All statistical calculations were performed with the SPSS 17 software

Results

Table 1 presents the main results of the $K_{a,e}$, AK at image detector (in fact, these values were measured at the anti-scatter grid entrance that was not removed during the experiment) and the image quality parameters for the images recorded in 1,024×1,024 matrix size 10 bits, 1,024×1,024 pixels 8 bits, 512×512 pixels 10 bits, and 512×512 pixels 8 bits, respectively.

Figure 2 shows the $K_{a,e}$, CNR and HCSR parameters for the different thicknesses of PMMA used in our experiment (from 16 to 28 cm) normalized to their values with 20 cm of PMMA thickness, in the best image quality offered by the X-ray system (1,024×1,024 pixels and 10 bits).

Figure 3 shows values of numerical parameters used to evaluate the image quality (CNR and HCSR) for the four available metrics and their variation with the different thicknesses of PMMA used in our experiment (from 16 to 28 cm).

In Table 1 and Fig. 2, $K_{a,e}$ at PMMA phantom per cine frame is seen to increase roughly at a factor of 2 when we increase the PMMA thickness by 4 cm (from 16 to 20, then to 24 and finally to 28 cm), while the AK at the entrance of the FD (in fact, the entrance at the anti-scatter grid) remains

Table 1 Numerical parameters: entrance surface air kerma at PMMA phantom ($K_{a,e}$), air kerma at flat detector (AK), contrast-to-noise ratio (CNR) as defined in Eq. 1 and high contrast image resolution (HCSR) as defined in Eq. 2 for cine mode and all PMMA thicknesses and field of view (FOV) of 25 cm

Numerical parameters	Matrix size and bits depth	16 cm of PMMA	20 cm of PMMA	24 cm of PMMA	28 cm of PMMA
kVp/mA		67/430	71/620	75/854	86/833
$K_{a,e}$ (μGy/fr)		143.6	290.5	586.8	964.8
AK at flat detector (μGy/fr)		0.732	0.734	0.745	0.685
CNR	1,024 and 10 bits	4.2±0.4	3.1±0.2	2.3±0.2	1.81±0.03
	1,024 and 8 bits	4.2±0.3	3.1±0.1	2.36±0.06	1.76±0.02
	512 and 10 bits	5.4±0.3	3.8±0.1	3.1±0.3	2.28±0.08
	512 and 8 bits	5.3±0.4	3.72±0.09	3.0±0.3	2.3±0.2
HCSR	1,024 and 10 bits	0.46±0.02	0.335±0.007	0.24±0.01	0.145±0.003
	1,024 and 8 bits	0.45±0.01	0.338±0.007	0.24±0.01	0.144±0.005
	512 and 10 bits	0.34±0.01	0.262±0.008	0.191±0.013	0.122±0.002
	512 and 8 bits	0.356±0.008	0.259±0.003	0.19±0.01	0.119±0.004

practically constant (4% of SD), thus showing that the automatic exposure control works properly. Simultaneously, the CNR decreased in a factor of 2.35 on average over all image formats, with 0.03 SD, which tends to show that this reduction is practically independent of the image format. The HCSR parameter decreases in a factor of 3.0 on average for the four image metrics presented, with an SD of 0.2. These results show that, when the patient thickness increases, the automatic brightness control, in order to maintain the image quality, requires higher doses. So to avoid high skin-dose rates, photon energy (i.e., the kV) was increased, thus causing appreciable decreases in CNR and HCSR and therefore loss of image quality.

When the matrix size is changed from 1,024×1,024 to 512×512 and the bits depth is kept unaltered, comparison of the different metrics (Table 1 and Fig. 3) shows an average improvement for all phantom thicknesses of 27% (±4%, Tukey's $p \leq 0.03$) in CNR. This is basically due to noise reduction (denominator) in Eq. 1 for CNR (the pixel mean values remain practically identical). This result demonstrates that the algorithm used by Philips to reduce the matrix size works like a low pass filter and is also in accordance with the one previously obtained by Vano et al. [8] for Siemens machines. The small SD suggests that there is no dependence of phantom thickness in CNR variation when the matrix size is changed. No significant variation has been found when the bits depth was reduced from 10 to 8 bits with a fixed matrix size.

The HCSR parameter underwent a reduction when the matrix size was reduced from 1,024×1,024 to 512×512; in this case, reductions as high as −25% were detected when the phantom thickness was 16 cm, the lowest variation being of −17% when the thickness was 28 cm (Tukey's p=0.01). This could be mainly due to a higher influence of the scatter radiation at a phantom thickness of 28 cm. The HCSR parameter seemed to remain unaffected by the bits depth variation (0±2%). As the definition of HCRS has changed since Vano et al.'s first paper [8], no comparison can be made in terms of degradation of HSCR.

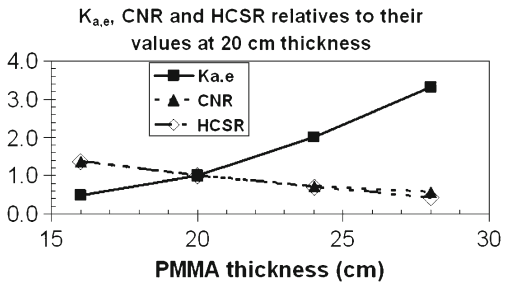

Fig. 2 Relative values to the ones at PMMA thickness of 20 cm for $K_{a,e}$, CNR and HCSR with the best image resolution of 1,024×1,024×8. The uncertainties were of 5% for $K_{a,e}$, and ≤10% for CNR and HCSR, and are not represented in the figure

Conclusions

The HCSR parameter, as defined in this paper, could prove useful in the investigation of the variations in HCSR properties in digital images obtained under different conditions

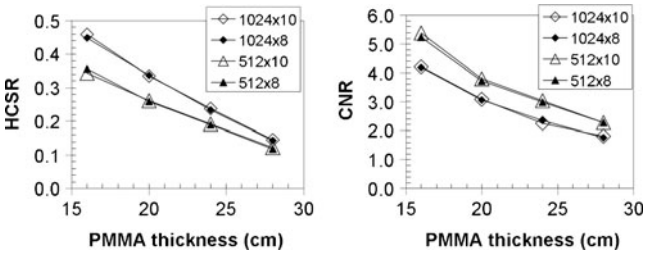

Fig. 3 For the four storage formats investigated in this work, on the left the HCSR and on the right the CNR. The uncertainties were ≤10% and are not represented in the figure

(e.g., with different PMMA thicknesses) even if the pixel values are rescaled by the changes on bit depth. It has been verified that when a degradation of HCSR is detected visually, the proposed parameter enables us to quantify numerically this degradation. With this simple mathematical formulation such as the HCSR parameter, DICOM images used in cardiology prove to undergo appreciable degradation in HCSR when the matrix size is reduced from 1,024×1,024 to 512×512 to reduce their storage size. This can be summarized as a loss of high frequency elements as reported in the case of lossy compression [5]. This image degradation has been observed on a test object with different PMMA phantom thicknesses in a setup simulating clinical practice. Moreover, the parameters investigated did not undergo significant variation when bits depth was reduced from 10 to 8 bits of grey scale; this tends to suggest that the reduction in bits depth could be managed without risk of losing patient's information, yet this must be achieved with an appropriate algorithm and specific noise properties according to Chuang and Huang [7]. These variations should be taken into account and, like in the case of jpg lossy compression algorithms, further investigations should be carried out to investigate a possible influence of matrix size and bits depth in real clinical images.

Acknowledgements The authors acknowledge the support of the Spanish grant SAF2009-10485 (Ministry of Science and Innovation). One of the authors (CU) acknowledges the support of the Direction of Research at Tarapaca University through senior research project No. 7713-10.

References

1. Elion JL: DICOM media interchange standards for cardiology: initial interoperability demonstration. Proc Annu Symp Comput Appl Med Care :591–595, 1995
2. Silber S, Dörr R, Zindler G, Mühling H, Diebel T: Impact of various compression rates on interpretation of digital coronary angiograms. Int J Cardiol 60:195–200, 1997
3. Brennecke R, Bürgel U, Simon R, Rippin G, Fritsch HP, Becker T, Nissen SE: American College of Cardiology/European Society of Cardiology International Study of Angiographic Data Compression Phase III: measurement of image quality differences at varying levels of data compression. J Am Coll Cardiol 35:1388–1397, 2000
4. Kerensky RA, Cusma JT, Kubilis P, Simon R, Bashore TM, Hirshfeld Jr, JW, Holmes Jr, DR, Pepine CJ, Nissen SE: American College of Cardiology/European Society of Cardiology International Study of Angiographic Data Compression Phase I: The effect of lossy data compression on recognition of diagnostic features in digital coronary angiography. J Am Coll Cardiol 35:1370–1379, 2000
5. Nissen SE, Hirshfeld Jr, JW, Simon R: Introduction and background: the International Angiographic Compression study. J Am Coll Cardiol 35:1367–1369, 2000
6. Erickson BJ: Irreversible Compression of Medical Images. White Paper-Irreversible Compression of Medical Images. 2000. Available at: http://www.siimweb.org/WorkArea/showcontent.aspx?id=1208. Accessed on 17 August 2011
7. Chuang K, Huang HK: Assessment of noise in a digital image using the join-count statistic and the Moran test. Phys Med Biol 37:357–369, 1997
8. Vano E, Ubeda C, Geiger B, Martinez LC, Balter S: Influence of image metrics when assessing image quality from a test object in cardiac X-ray systems. J Digit Imaging 24:331–338, 2011
9. Rassow J, Schmaltz AA, Hentrich F, Streffer C: Effective doses to patients from paediatric cardiac catheterization. Br J Radiol 73:172–183, 2000
10. ICRU International Commission on Radiological Units and Measurements: Patient dosimetry for x rays used in medical imaging ICRU Report 74. J. ICRU 5(2), 2005
11. Perry et al: European guidelines for quality assurance in breast cancer screening and diagnosis. Fourth edition. ISBN 92-79-01258-4, 2006
12. Gagne RM, Boswell JS, Myers KJ: Signal detectability in digital radiography: spatial domain figures of merit. Med Phys 30:2180–2193, 2003
13. Muhogora WE, Devetti A, Padovani R, Msaki P, Bonutti F: Application of European protocol in the evaluation of contrast-to-noise ratio and mean glandular dose for two digital mammography systems. Radiat Prot Dosim 129:231–236, 2008